



# A small peptide inhibits siRNA amplification in plants by mediating autophagic degradation of SGS3/RDR6 bodies

Xin Tong<sup>1</sup>, Song-Yu Liu<sup>1</sup>, Jing-Ze Zou<sup>1</sup>, Jia-Jia Zhao<sup>1</sup>, Fei-Fan Zhu<sup>1</sup>, Long-Xiang Chai<sup>1</sup>, Ying Wang<sup>2</sup>, Chenggui Han<sup>2</sup>  & Xian-Bing Wang<sup>1,\*</sup> 

## Abstract

Selective autophagy mediates specific degradation of unwanted cytoplasmic components to maintain cellular homeostasis. The suppressor of gene silencing 3 (SGS3) and RNA-dependent RNA polymerase 6 (RDR6)-formed bodies (SGS3/RDR6 bodies) are essential for siRNA amplification in plants. However, whether autophagy receptors regulate selective turnover of SGS3/RDR6 bodies is unknown. By analyzing the transcriptomic response to virus infection in *Arabidopsis*, we identified a virus-induced small peptide 1 (VISP1) composed of 71 amino acids, which harbor a ubiquitin-interacting motif that mediates interaction with autophagy-related protein 8. Overexpression of VISP1 induced selective autophagy and compromised antiviral immunity by inhibiting SGS3/RDR6-dependent viral siRNA amplification, whereas *visp1* mutants exhibited opposite effects. Biochemistry assays demonstrate that VISP1 interacted with SGS3 and mediated autophagic degradation of SGS3/RDR6 bodies. Further analyses revealed that overexpression of VISP1, mimicking the *sgs3* mutant, impaired biogenesis of endogenous trans-acting siRNAs and up-regulated their targets. Collectively, we propose that VISP1 is a small peptide receptor functioning in the crosstalk between selective autophagy and RNA silencing.

**Keywords** autophagy; peptide; plant virus; RNA silencing; SGS3

**Subject Categories** Plant Biology; RNA Biology

DOI 10.15252/embj.2021108050 | Received 17 February 2021 | Revised 20 May 2021 | Accepted 27 May 2021 | Published online 22 June 2021

The EMBO Journal (2021) 40: e108050

## Introduction

Macroautophagy called autophagy is a conserved macromolecule degradation pathway in eukaryotes. In plants, autophagic degradation is a highly regulated process to maintain cell homeostasis in plant development and stress responses (Signorelli *et al.*, 2019). During autophagic processes, a double-membrane autophagosome is formed to sequester and deliver aggregated proteins and damaged

organelles into vacuoles for degradation (Wang *et al.*, 2018). More than 30 autophagy-related genes (*ATG*) have been identified in *Arabidopsis* (Wang *et al.*, 2018). Among these components, ATG8/LC3 family proteins are central players in autophagosome formation and cargo recruitment (Noda *et al.*, 2010). After being modified with the lipid phosphatidylethanolamine (PE), the resulting ATG8-PE decorates autophagic membranes and provides cargo docking sites for autophagic degradation (Noda *et al.*, 2010). During selective autophagy, autophagic receptors provide linkages between specific cargos and ATG8 (Marshall & Vierstra, 2018). ATG8-binding adaptors and receptors contain hydrophobic pockets with a motif W/F/Y-X-X-L/I/V, termed ATG8-interacting motif (AIM) (Noda *et al.*, 2010). Recently, proteins harboring a ubiquitin-interacting motif (UIM) were identified as new class of receptors and adaptors (Marshall *et al.*, 2015; Marshall *et al.*, 2019). Currently, studies about UIM motif-containing cargo receptors are very limited. Thus, exploring new UIM motif-containing autophagy receptors will permit a better understanding of selective autophagy in plants.

Selective autophagy is stimulated by abiotic stresses and microbial pathogen infections (Signorelli *et al.*, 2019; Yang *et al.*, 2020). For instance, mammalian proteins p62/SQSTM1 and NBR1 not only are selective autophagy substrates, but also act as cargo receptors for degradation of ubiquitinated substrates (Pankiv *et al.*, 2007; Kirkin *et al.*, 2009). The *Arabidopsis* NBR1 is a functional hybrid of mammalian p62 and NBR1 (Svenning *et al.*, 2011) and targets ubiquitinated protein aggregates for degradation in stress responses (Zhou *et al.*, 2013). Plant-specific ATG8-interacting protein 1 (ATI1) mediates the trafficking of plastid proteins to the vacuole via autophagy-dependent machinery (Michaeli *et al.*, 2014). Moreover, three close-related dicot-specific ATI proteins interact with UBAC2 proteins (ubiquitin-associated [UBA] protein 2) for mediating autophagy of specific ER components (Zhou *et al.*, 2018).

RNA silencing is a conserved antiviral mechanism in eukaryotic organisms. During antiviral RNA silencing, host Dicer and argonaute proteins are core silencing components for biogenesis of virus-derived small interfering RNAs (vsiRNAs) and RNA slicing, respectively (Guo *et al.*, 2019). Furthermore, host RDRs can amplify secondary siRNA and increase antiviral RNA-silencing potency

<sup>1</sup> State Key Laboratory of Agro-Biotechnology, College of Biological Sciences, China Agricultural University, Beijing, China

<sup>2</sup> College of Plant Protection, China Agricultural University, Beijing, China

\*Corresponding author. Tel: +86 10 62733313; E-mail: wangxianbing@cau.edu.cn

through dsRNA synthesis (Wang *et al*, 2010). A plant-specific RNA-binding protein, SGS3, is a functional partner of RDR6, and they form SGS3/RDR6 bodies for siRNA amplification (Mourrain *et al*, 2000; Peragine *et al*, 2004). *Cucumber mosaic virus* (CMV) is one of the most important viruses causing severe symptoms in crops. The CMV-encoded 2b protein is a strong viral suppressor of RNA silencing (VSR) (Diaz-Pendon *et al*, 2007). To rule out interference of 2b in antiviral silencing, 2b-deficient mutant viruses were used to screen new antiviral components (Guo *et al*, 2017; Guo *et al*, 2018). For instance, an alanine substitution mutant of CMV 2b in the 15<sup>th</sup> leucine and 18<sup>th</sup> methionine (CMV-2blm) is less virulent than wild-type CMV due to its deficiency in suppressing RDR6/SGS3-dependent RNA silencing (Dong *et al*, 2016).

Most of the characterized antimicrobial peptides are derived from long unfunctional precursor proteins (Olsson *et al*, 2018). However, very few studies characterize small peptides directly translated from small open reading frames (sORFs, 30-100 amino acids) (Tavormina *et al*, 2015). Here, we identified a virus-induced small peptide 1 (VISP1) composed of 71 amino acids harboring an UIM to interact with ATG8. VISP1 serves as a selective autophagy cargo receptor to mediate autophagic degradation of SGS3/RDR6 bodies. Our results provide new insights into biological functions of a peptide cargo receptor in antiviral RNA silencing and autophagy.

## Results

### Characterization of an ATG8-interacting small peptide

To investigate cellular components functioning in plant-virus interactions, we examined transcriptome response of *Arabidopsis* plants to CMV infection. At 7 days post-inoculation (dpi), systemically infected leaves were harvested for RNA extraction and RNA-Seq. Compared with mock treatments, CMV infection induced expression of 261 genes by fourfold (FDR < 0.05), including 18 sORFs among the 7,901 predicted sORFs in a previous study (Fig 1A) (Hanada *et al*, 2013). The virus-induced 18 sORFs are derived from protein coding regions, rRNA genes, and intergenic regions (Fig 1A and Appendix File S1). Here, these small peptides were tentatively named virus-induced small peptides (VISPs). RT-qPCR assays revealed that the *VISP1-12* mRNAs were significantly induced by CMV infection (Appendix Fig S1A). BLAST analyses show that *VISP1-18* has low similarities in amino acid sequences, but some VISPs share same amino acid sequences although they are from different loci (Appendix Fig S1B and File S1), indicating gene duplications in these loci as described previously (De Smet *et al*, 2017). Given that the *VISP1* mRNA was significantly induced by CMV infection at 7, 14, and 21 dpi (Appendix Fig S1C), the uncharacterized *VISP1* peptide was selected for further analyses in this study.

The *VISP1* ORF encodes a putative 71-amino acid peptide in the gene locus *AT1G21525*. CMV-2blm and CMV infection resulted in increased accumulation of *VISP1* (*AT1G21525*) by 10.2- and 8.8-fold compared with mock treatments (Appendix Fig S2A, *P*-value < 0.05). To determine whether the *VISP1* can be translated in vivo, the *VISP1* genomic fragment from 3,000 bp upstream of the start codon to the end of the ORF was in-frame fused to the N terminus of  $\beta$ -glucuronidase (GUS) (*VISP1<sup>PRO</sup>::VISP1-GUS*). GUS staining assays revealed that *VISP1-GUS* accumulated to low levels

in mock-treated *VISP1<sup>PRO</sup>::VISP1-GUS* transgenic plants, but was induced obviously after CMV-2blm infection (Fig 1B and Appendix Fig S2B). In contrast, *VISP1<sup>PRO</sup>::VISP1<sup>TGA</sup>-GUS*, containing a TGA after the *VISP1* ORF, served as a negative control and could not express GUS in transgenic plants (Fig 1B and Appendix Fig S2D). Moreover, the *VISP1-GUS* fusion protein was immunoprecipitated with GUS-specific antibodies and analyzed by liquid chromatography-tandem mass spectrometry (LC-MS/MS). As expected, two peptides were derived from the N terminal *VISP1* fragment (Appendix Fig S2E and F, and G). Collectively, these results indicate that *VISP1* is translated in vivo and induced by virus infection.

BLAST analyses reveal that *VISP1* orthologues are present in Brassicaceae plants (Appendix Fig S3). *VISP1* orthologues shared high similarities in amino acid sequences (Fig 1C). Intriguingly, a conserved motif (<sup>39</sup>IISALXPS<sup>46</sup>, X represent any amino acid) of *VISP1* orthologues is reminiscent of the ubiquitin-interacting motif (UIM) ( $\psi$ - $\zeta$ -X-A- $\psi$ -X-X-S;  $\psi$ , small hydrophobic residues;  $\zeta$ , hydrophilic residues; X, any amino acid) that is a consensus motif in newly identified ATG8-interacting receptors or adaptors (Marshall *et al*, 2019). In addition, *VISP1* orthologues have another conserved sequence (<sup>28</sup>RKLVK<sup>32</sup>) that harbors three basic amino acid residues (arginine/lysine) (Fig 1C), termed arginine/lysine-rich motif (ARM).

Given that *VISP1* harbors a ATG8-interacting domain, we next examined whether *VISP1* interacted with ATG8 using biomolecular fluorescence complementation (BiFC) assays. Among the nine ATG8 (ATG8a-i) isoforms encoded by *Arabidopsis* genome, ATG8a and ATG8f were selected for BiFC assays. We first fused the coding sequences of *Arabidopsis* ATG8a and ATG8f to the N halves of YFP (Y<sup>N</sup>). The coding sequence of *VISP1* was fused to the C halves of YFP (Y<sup>C</sup>). Co-expression of *VISP1*-Y<sup>C</sup> with Y<sup>N</sup>-ATG8a or Y<sup>N</sup>-ATG8f resulted in reconstitution of YFP fluorescence in *N. benthamiana* leaves at 60 h post-inoculation (hpi) (Fig 1D). In contrast, co-expression of negative control combinations failed to produce YFP signal, although all proteins were expressed (Appendix Fig S4). The <sup>39</sup>IISALXPS<sup>46</sup> motif of *VISP1*-Y<sup>C</sup> was replaced with <sup>39</sup>DISDDXPD<sup>46</sup>, termed *VISP1<sup>mUIM</sup>-Y<sup>C</sup>*. Co-expression of *VISP1<sup>mUIM</sup>-Y<sup>C</sup>* and Y<sup>N</sup>-ATG8a failed to produce YFP signal (Fig 1D), indicating that the UIM motif is essential for the *VISP1*-ATG8 interaction, whereas *VISP1<sup>mARM</sup>-Y<sup>C</sup>* harboring substitution of <sup>28</sup>RKLVK<sup>32</sup> motif of *VISP1* with <sup>28</sup>AALVA<sup>32</sup> produced YFP signal when co-expressed with Y<sup>N</sup>-ATG8a (Appendix Fig S4A), indicating that the ARM motif is not required for the *VISP1*-ATG8 interaction.

Co-immunoprecipitation (Co-IP) assays were performed to determine the *VISP1*-ATG8 interaction in vivo. The Flag-ATG8a fusion protein was co-expressed transiently with GFP, *VISP1*-GFP, or *VISP1<sup>mUIM</sup>-GFP* by agroinfiltration. Infiltrated leaves were treated with 2 mM 3-MA to inhibit autophagic degradation at 48 hpi and then harvested for Co-IP assays 12 h later. The results revealed that Flag-ATG8a was precipitated with *VISP1*-GFP, but not with *VISP1<sup>mUIM</sup>-GFP* or GFP (Fig 1E). In vitro pull-down assays were performed to determine the direct *VISP1*-ATG8 interaction. The *VISP1*-His or *VISP1<sup>mUIM</sup>-His* proteins were incubated with the GST-ATG8a, GST-*VISP1*, or GST proteins and precipitated with anti-GST beads. Western blotting assays revealed that the *VISP1*-His protein was precipitated with GST-ATG8a but not with GST (Fig 1F). In contrast, *VISP1<sup>mUIM</sup>-His* was not co-precipitated with GST-*VISP1* (Fig 1F).

Collectively, these results suggest that *VISP1* is a virus-induced small peptide harboring a conserved ATG8-interacting UIM motif in

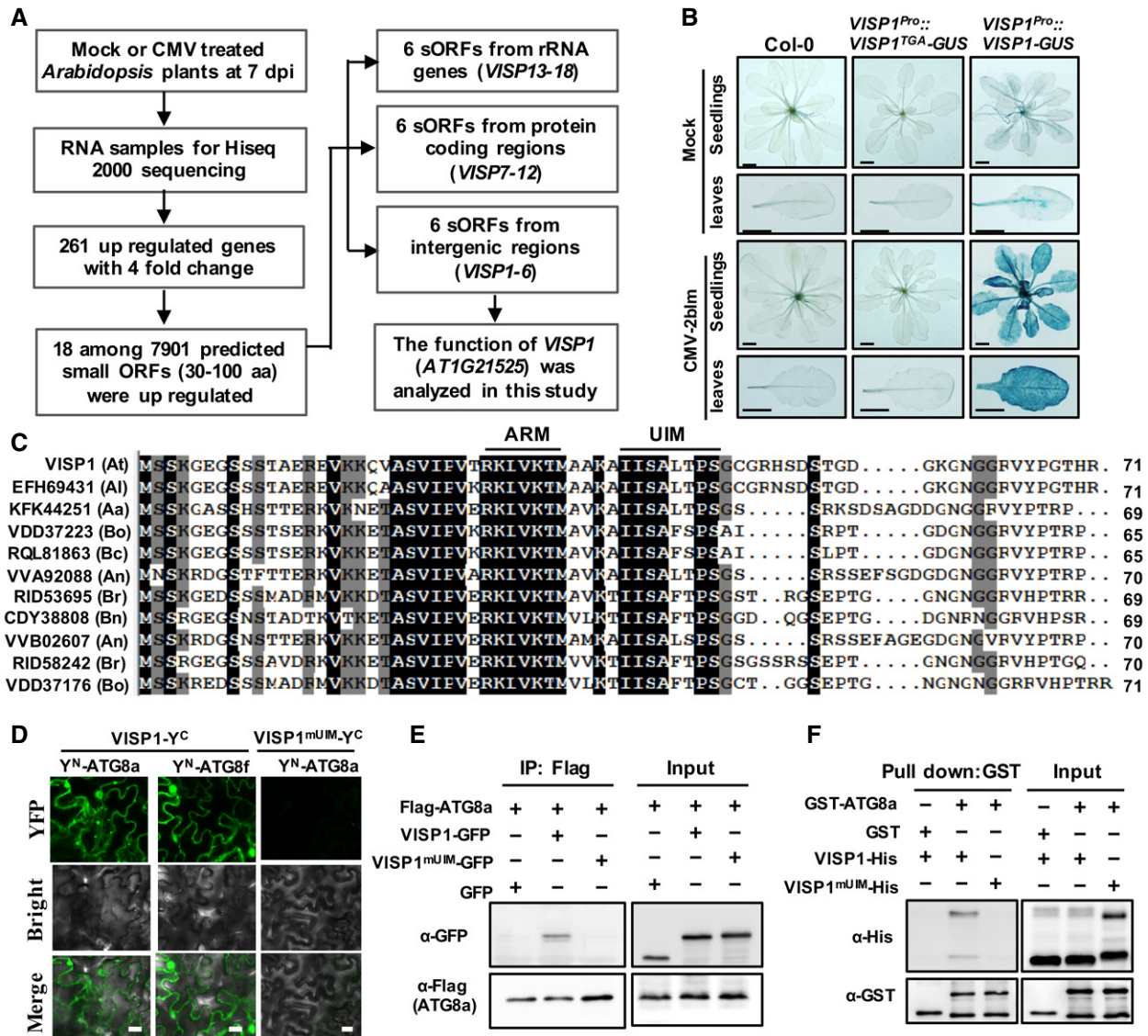


**Figure 1. Characterization of an ATG8-interacting small peptide.**

A Work flow to identify virus-induced small peptides in *Arabidopsis*.

B GUS activity of *VISP1<sup>Pro</sup>::VISP1-GUS* transgenic *Arabidopsis* plants infected by mock buffer or CMV-2blm at 7 dpi. Scale bar = 5 mm.

C Amino acid sequence alignment of AtVISP1 and its homologues from *Arabidopsis lyrata* (Al), *Brassica rapa* (Br), *Brassica napus* (Bn), *Brassica oleracea* (Bo), *Brassica cretica* (Bc), *Arabis alpine* (Aa), and *Arabis nemorensis* (An). The conserved ubiquitin-interacting motif (UIM) and arginine/lysine-rich motif (ARM) are indicated by lines.

D BiFC analysis of interactions between VISP1 or VISP1<sup>mUIM</sup> and ATG8a or ATG8f in *N. benthamiana* leaves. Images were taken at 60 hpi. Scale bar = 20  $\mu$ m.

E Co-IP experiments examining protein interactions between ATG8a with VISP1 or VISP1<sup>mUIM</sup>. *N. benthamiana* leaves were agroinfiltrated and treated with 2 mM 3-MA at 48 hpi and then for IP with anti-Flag beads 12 h later.

F GST pull-down analysis of the interactions between ATG8a with VISP1 or VISP1<sup>mUIM</sup>.

Source data are available online for this figure.

*Arabidopsis* and that VISP1 can interact with ATG8 in vivo and in vitro.

### Overexpression of VISP1 induces autophagosome formation and selective autophagy

Given the VISP1–ATG8 interaction, we next investigated whether VISP1 induced selective autophagy. To this end, we

generated transgenic *Arabidopsis* plants overexpressing VISP1-Flag, VISP1<sup>mUIM</sup>-Flag, and VISP1<sup>mARM</sup>-Flag, under control of the cauliflower mosaic virus (CaMV) 35S promoter in the Col-0 background. To visualize autophagy induction by VISP1 overexpression, we transformed the autophagosomal marker YFP-ATG8e (Zhuang *et al*, 2013) into Col-0, VISP1<sup>OE1</sup>, and VISP1<sup>OE2</sup> plants. As shown in Fig 2A and B, a significantly increased puncta numbers of YFP-ATG8e were observed in YFP-ATG8e/VISP1<sup>OE</sup> cells compared with those of YFP-

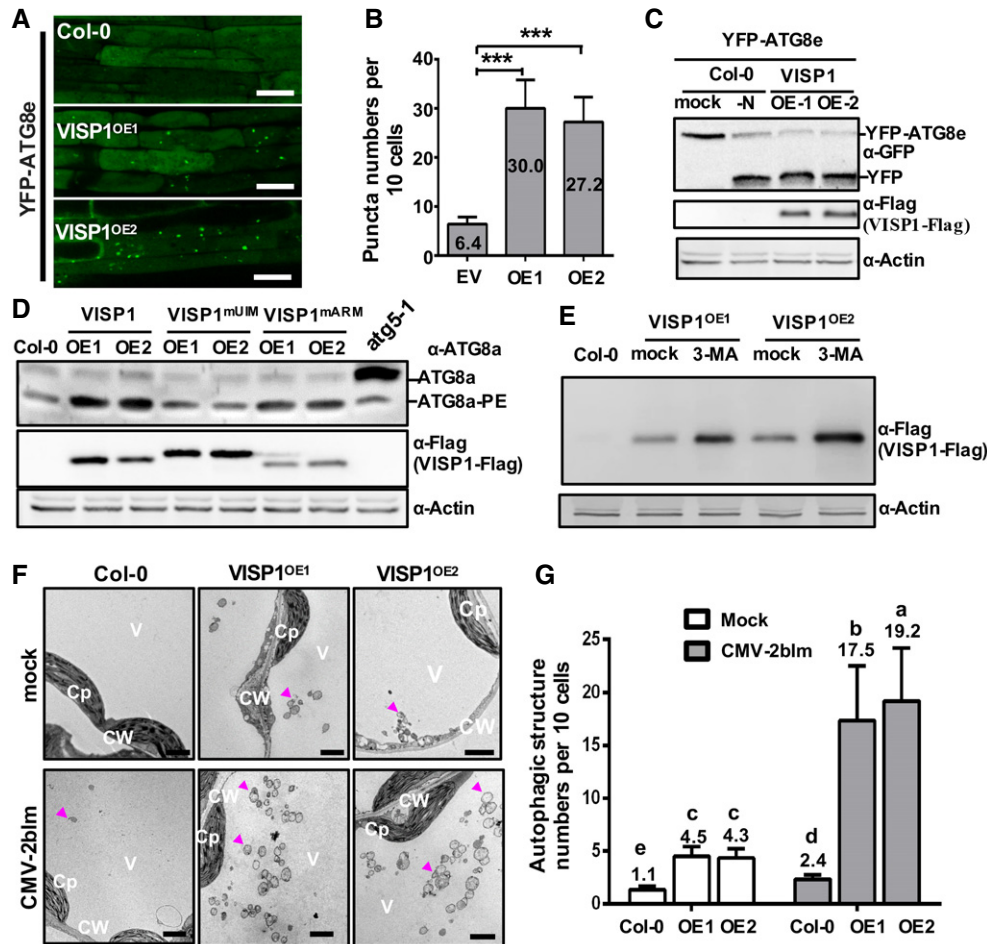


**Figure 2. Overexpression of VISP1 induced autophagy and autophagosome formation.**

- A Confocal microscopy of YFP-ATG8e-labeled autophagic bodies in root cells of YFP-ATG8e/Col-0 and YFP-ATG8e/VISP1<sup>OE</sup> plants. Seven-day-old seedlings were inoculated in liquid 1/2MS medium with 1  $\mu$ M ConA for 12 h in dark. Scale bar = 20  $\mu$ m.
- B Puncta numbers of YFP-ATG8e-labeled autophagic bodies per 10 cells in panel (A). Data points represent means of three biological repeats. Error bars indicate SD. \*\*\* $P < 0.001$  (Student's  $t$ -test).
- C Western blotting analysis of the vacuolar delivery of the free YFP protein in the plants as shown in panel (A). YFP-ATG8e/Col-0 plants were treated with N starvation as a positive control of autophagy induction. Total proteins were analyzed with GFP antibodies. Actin served as loading controls.
- D Western blotting analysis of accumulation of ATG8a and ATG8a-PE in leaves of 4-week-old Col-0, VISP1<sup>OE</sup>, VISP1<sup>M/UE</sup>, and VISP1<sup>M/UE</sup> plants.
- E Western blotting detecting accumulation of VISP1-Flag in 7-day-old Col-0 and VISP1<sup>OE</sup> seedlings. Seedlings were treated with 3-MA (10 mM) or buffer for 18 h at dark prior to protein detection.
- F Representative TEM images of autophagic structures in inoculated leaves of Col-0 and VISP1<sup>OE</sup> plants treated with mock buffer or CMV-2blm infection at 4 dpi. The leaves were treated with 1  $\mu$ M ConA at 4 dpi for 12 h in dark before TEM sampling. Magenta arrowheads indicate autophagic bodies inside the vacuoles. Scale bar = 2  $\mu$ m. Cp, chloroplast; CW, cell wall; V, vacuole.
- G Autophagic structure numbers per 10 cells in panel (F). Error bars indicate SD. Letters indicate significant differences (ANOVA,  $P < 0.05$ ).

Source data are available online for this figure.

ATG8e/Col-0. We further performed YFP-ATG8e processing assays to confirm induced autophagy activity by VISP1<sup>OE</sup>. Upon autophagy induction, the YFP-ATG8e protein is degraded into free YFP and the YFP level reflects the induction level of autophagy. Immunoblot analysis showed that free YFP accumulated in YFP-ATG8e/VISP1<sup>OE</sup> plants but absent in YFP-ATG8e/Col-0 plants (Fig 2C). As a positive control of autophagy induction, treatment with nitrogen starvation induced production of free YFP in YFP-ATG8e/Col-0 plants (Fig 2C). These results indicate overexpression of VISP1 induces selective autophagy in *Arabidopsis*.

The conjugation of ATG8 to phosphatidylethanolamine (PE) occurs during autophagosome formation (Ichimura *et al*, 2000). Western blotting results showed that accumulation of ATG8a-PE in leaves of 4-week-old VISP1<sup>OE</sup> and VISP1<sup>M/UE</sup> plants is higher than that of wild-type Col-0 plants, but VISP1<sup>M/UE</sup> plants accumulated comparable levels of ATG8a-PE with Col-0 plants (Fig 2D). As a negative control, large amount of free ATG8a accumulated and PE modification was almost abolished in the *atg5-1* mutant plants that have been shown to be autophagy-deficient mutants in previous studies (Thompson *et al*, 2005) (Fig 2D). Furthermore, 3-MA

treatment improved accumulation of the VISP1-Flag protein in VISP1<sup>OE1</sup> and VISP1<sup>OE2</sup> plants (Fig 2E), indicating that VISP1 was degraded by selective autophagy. These results indicate that overexpression of VISP1 and VISP1<sup>mARM</sup>, but not VISP1<sup>mUIM</sup>, induces ATG8 conjugation and selective autophagy.

To further determine autophagy induction by VISP1 overexpression, autophagy activity in leaves of 4-week-old Col-0, VISP1<sup>OE1</sup>, and VISP1<sup>OE2</sup> plants was monitored by transmission electron microscopy (TEM). Compared with Col-0 plants, VISP1<sup>OE1</sup> and VISP1<sup>OE2</sup> harbored much more autophagic structures in vacuoles (Fig 2F and G). Similarly, TEM assays revealed that overexpression of VISP1-Flag induced production of autophagic structures in *N. benthamiana* leaves (Appendix Fig S5A and B). Overexpression of VISP1-Flag, rather than VISP1<sup>mUIM</sup>-Flag, induced CFP-NbATG8f-labeled autophagosomes in *N. benthamiana* leaves (Appendix Fig S5C and D).

In TEM assays, autophagic structures were induced by approximately twofold in Col-0 plants after inoculation with CMV-2blm at 4 dpi (Fig 2F and G). Furthermore, virus-infected VISP1<sup>OE</sup> leaves produced large amounts of autophagic structures and induced autophagy activity by about 16-fold compared with healthy Col-0 plants (Fig 2F and G). In consistence, MDC staining results revealed that CMV infection resulted in increased autophagosome numbers in Col-0 and VISP1<sup>OE1</sup> leaves (Appendix Fig S6A and B). Transient

expression of the autophagosomal marker YFP-ATG8e could label autophagic bodies in *N. benthamiana* leaves. CMV infection resulted in a significantly increased puncta number of YFP-ATG8e compared with the mock buffer treatment (Appendix Fig S6C and D).

To further determine whether CMV infection induces autophagy in *Arabidopsis*, RT-qPCR assays were carried out to detect accumulation of *ATG5*, *ATG8a*, and *ATG9* that have been shown to be involved in autophagy pathway (Thompson *et al*, 2005; Noda *et al*, 2010; Zhuang *et al*, 2017). The results revealed that accumulation of *ATG5*, *ATG8a*, and *ATG9* mRNAs was significantly induced by CMV infection in *Arabidopsis* (Appendix Fig S6E).

Collectively, we have presented multiple lines of evidence showing that overexpression of VISP1 and CMV infection induces selective autophagy.

### Overexpression of VISP1 inhibits amplification of viral siRNA and antiviral immunity

We next investigated the VISP1 functions in plant virus infection. To this end, Col-0 and VISP1<sup>OE</sup> plants were inoculated with CMV-2blm. Besides, the *sgs3-1* and *rd6-15* mutants served as susceptible controls due to their defective vsiRNA amplification (Mourrain *et al*, 2000; Peragine *et al*, 2004). Compared with Col-0 plants, VISP1<sup>OE</sup>

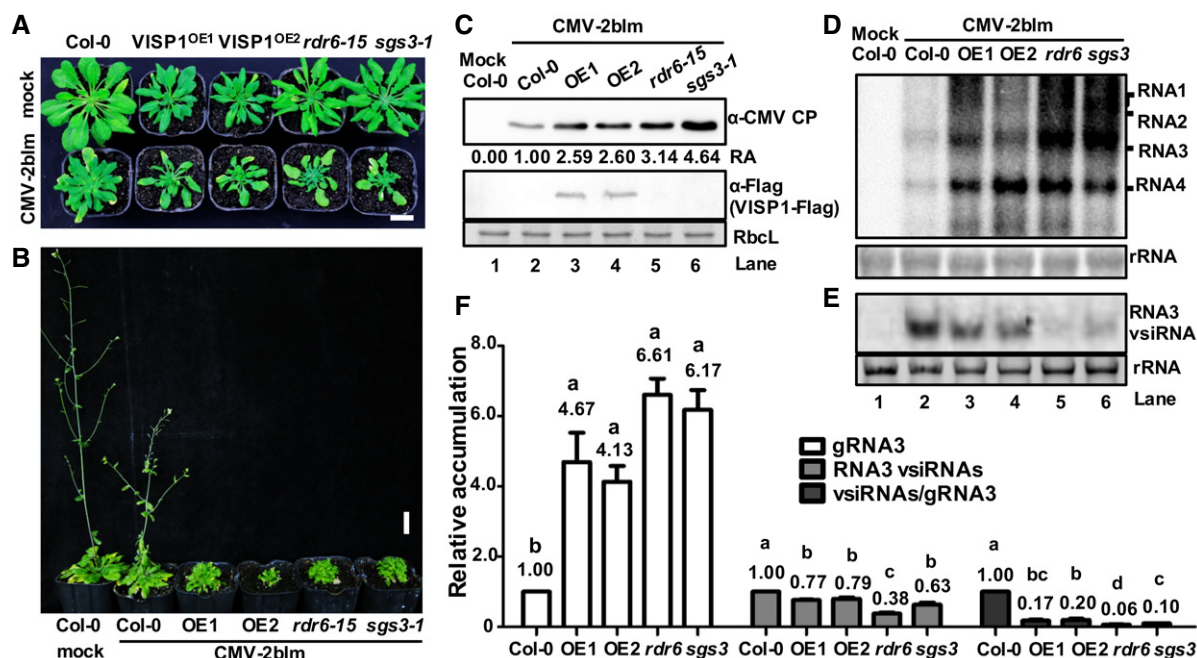
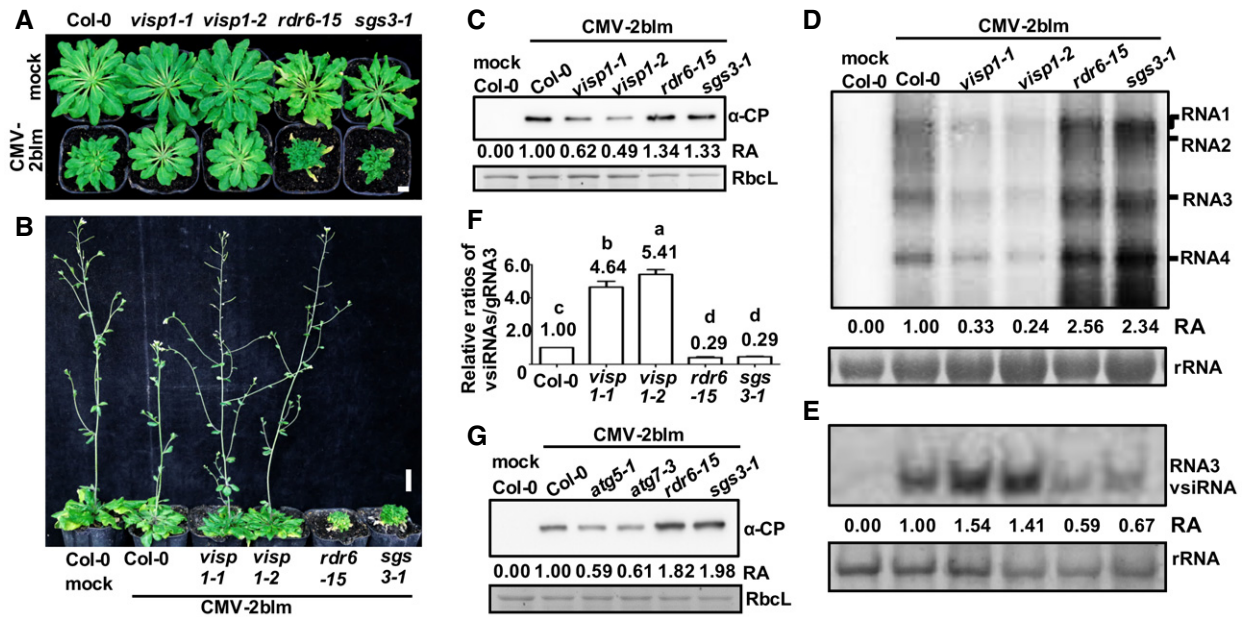


**Figure 3. Overexpression of VISP1 promotes CMV infection by inhibiting vsiRNA amplification.**

- A Development and pathogenic responses of Col-0, VISP1<sup>OE1</sup>, VISP1<sup>OE2</sup>, *rd6-15*, and *sgs3-1* plants to mock buffer or CMV-2blm infection at 21 dpi. Scale bar = 2 cm.  
 B Long-term symptoms of Col-0, VISP1<sup>OE1</sup>, VISP1<sup>OE2</sup>, *rd6-15*, and *sgs3-1* plants inoculated with CMV-2blm at 50 dpi. Scale bar = 2 cm.  
 C Western blotting showing accumulation of CMV CP and VISP1-Flag in systemically infected leaves at 14 dpi. Relative accumulation (RA) of CMV CP was calculated from band densities. Rubisco complex large subunit (RbcL) served as loading controls.  
 D Northern blotting analyzing accumulation of genomic RNAs (gRNAs) in systemically leaves of Col-0, OE1 (VISP1<sup>OE1</sup>), OE2 (VISP1<sup>OE2</sup>), *rd6-15*, and *sgs3-1* plants infected by CMV-2blm at 14 dpi. Methylene blue-stained rRNA were used as loading controls.  
 E Northern blotting analyzing accumulation of RNA3-derived vsiRNAs in the same samples as shown in panel (D).  
 F Relative accumulation of gRNA3, RNA3-derived vsiRNA, and vsiRNAs/gRNA3 ratios calculated from hybridization signal intensities of northern blotting in (D, E). Values in Col-0 plants were set as 1. Data points represent means of three biological repeats. Error bars indicate SD. Letters indicate significant differences (ANOVA,  $P < 0.05$ ).

Source data are available online for this figure.



plants, *sgs3-1* and *rdr6-15* mutants developed more severe symptoms at 21 dpi and 50 dpi (Fig 3A and B). Consistently, western blotting detected higher levels of the CMV CP protein in *VISP1<sup>OE1</sup>*, *VISP1<sup>OE2</sup>*, *sgs3-1*, and *rdr6-15* plants than in Col-0 plants (Fig 3C). Similarly, *VISP1<sup>OE</sup>* plants exhibited compromised resistance against TuMV-GFP, a turnip mosaic virus (TuMV) containing a GFP insertion (Appendix Fig S7A and B). Furthermore, expression of VISP1 in potato virus X (PVX) vector facilitated PVX infection (Appendix Fig S7C and D). These results indicate that overexpression of VISP1 compromises antiviral immunity against several RNA viruses.

Northern blotting was performed to assess accumulation of viral genomic RNAs (gRNAs) and virus-derived siRNAs (vsRNAs) in systemically infected leaves. Intriguingly, *VISP1<sup>OE</sup>* plants, like *sgs3-1* and *rdr6-15* mutants, contained higher levels of viral gRNAs and lower levels of vsRNAs compared with Col-0 plants (Fig 3D and E). Hybridization signal intensities of viral gRNA3 and RNA3-derived vsRNAs were evaluated to compare accumulation of viral gRNAs and vsRNAs, respectively. The results revealed that the gRNA3 levels in *VISP1<sup>OE</sup>* were at least fourfold those of infected Col-0 plants (Fig 3F,  $P$ -value  $< 0.05$ ), while *VISP1<sup>OE</sup>* plants only accumulated to 80% of vsRNAs compared with Col-0 plants (Fig 3F,  $P$ -value  $< 0.05$ ). Furthermore, we compared the relative RNA3-vsiRNAs/gRNA3 ratios that represent vsRNA amplification efficiency in different

plants. The results revealed that the RNA3-vsiRNAs/gRNA3 ratios in *VISP1<sup>OE</sup>* plants reduced to 20% of those of Col-0 plants (Fig 3F,  $P$ -value  $< 0.01$ ). Similarly, the RNA3-vsiRNAs/gRNA3 ratios in *rdr6-15* and *sgs3-1* mutants reduced to 10% of those of Col-0 plants (Fig 3F,  $P$ -value  $< 0.01$ ). Therefore, these results suggest that VISP1 overexpression negatively regulates vsRNA amplification.

#### VISP1 knockout mutants exhibit enhanced antiviral immunity

We generated loss-of-function *visp1* mutations using the CRISPR/Cas9 system. The resulting *visp1-1* and *visp1-2* contain two different deletions in the VISP1 ORF region (Appendix Fig S8). Upon challenged by CMV-2blm, *visp1-1* and *visp1-2* mutants exhibited much milder virus symptoms at 21 dpi compared with Col-0 plants (Fig 4A). Notably, *visp1-1* and *visp1-2* plants did not exhibit observable symptoms at 50 dpi, in contrast with obviously stunting symptoms of Col-0 plants (Fig 4B). Western blotting with systemically infected leaves revealed strikingly lower levels of CMV CP in *visp1-1* and *visp1-2* mutants than in Col-0 plants (Fig 4C). Moreover, *visp1-1* and *visp1-2* mutants exhibited strong defense against CMV- $\Delta$ 2b and TuMV-GFP infections (Appendix Fig S9). Collectively, these results suggest that VISP1 knockout mutants exhibit resistance to plant viruses.

Northern blotting showed that strikingly decreased levels of viral gRNAs but higher levels of vsRNAs accumulated in *visp1-1* and *visp1-2* plants than in Col-0 plants (Fig 4D and E). Comparative analyses from hybridization signal intensities revealed that the RNA3-vsRNAs/gRNA3 ratios increased by at least fourfold in *visp1* mutants compared with Col-0 plants (Fig 4F). As described above, *rdr6-15* and *sgs3-1* mutant plants were defective in vsRNA amplification and exhibited less virus resistance to CMV-2blm compared with Col-0 plants (Fig 4). Collectively, these results demonstrate that siRNA amplification is improved in *visp1* mutants.

We next examined whether autophagy affects CMV-2blm infection. The autophagy-related proteins ATG5 and ATG7 are essential for ATG8-lipid adduct and autophagosome formation (Marshall & Vierstra, 2018). The T-DNA insertion mutants, *atg5-1* (SAIL\_129\_B07) and *atg7-3* (SAIL\_11\_H07), have been shown to be completely defective in autophagy (Thompson et al, 2005; Lai et al, 2011; Luo et al, 2017). Inoculation assays showed that the *atg5-1* and *atg7-3* autophagy mutants allow lower accumulation of CMV CP in inoculated leaves than those of Col-0, *rdr6-15*, and *sgs3-1* plants at 4 dpi (Fig 4G), indicating that autophagy plays a negative

role in plant defense against CMV-2blm infection. Collectively, these results clearly suggest that the VISP1-mediated selective autophagy negatively regulates antiviral immunity.

### VISP1 interacts with SGS3 *in vivo* and *in vitro*

Given that VISP1 negatively regulates vsRNA amplification that have been shown to be dependent on the RDR6/SGS3 pathway (Wang et al, 2010; Dong et al, 2016), we speculated that VISP1 probably mediated selective autophagic degradation of SGS3 and/or RDR6. To test this hypothesis, we determined whether VISP1 interacted with SGS3 or RDR6 using BiFC assays. As expected, co-expression of SGS3-Y<sup>N</sup> and VISP1-Y<sup>C</sup> resulted in reconstitution of YFP fluorescence, while RDR6-Y<sup>N</sup>/VISP1-Y<sup>C</sup> and other negative controls failed to produce YFP signal (Fig 5A and Appendix Fig S10A). These results suggest that VISP1 interacts with SGS3 but not with RDR6.

The SGS3 protein contains a ZF domain, an XS domain, and a coiled-coil domain (CC), and the deletion mutants were fused to Y<sup>N</sup> for BiFC assays (Fig 5B). Moreover, the VISP1 UIM and ARM motifs

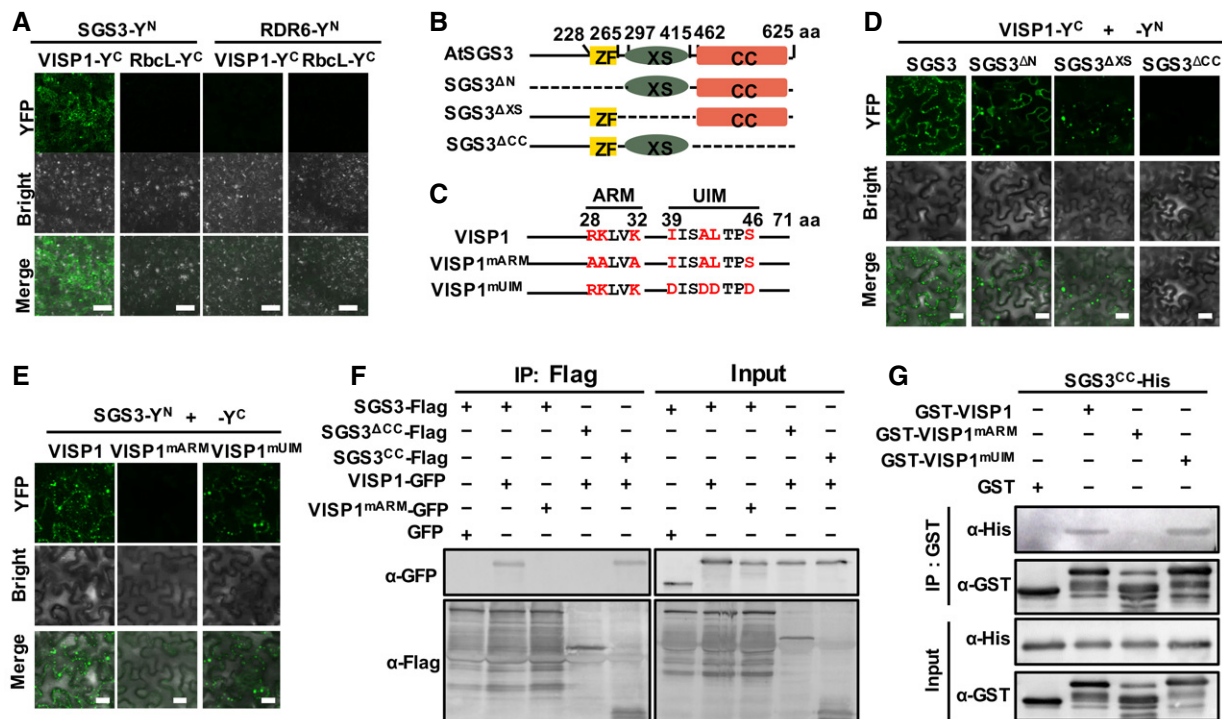


**Figure 5. VISP1 interacts with SGS3 *in vivo* and *in vitro*.**

A BiFC analyses of interactions between VISP1 and SGS3 or RDR6 in *N. benthamiana* leaves at 60 hpi. RbcL served as a negative control. Scale bar = 20 μm.  
 B Schematic representation of the *Arabidopsis* SGS3 protein and deletion mutants. Deleted regions are indicated by dashed lines. N: N terminus including zinc finger (ZF), XS: rice protein X and SGS3, CC: coiled-coil domain.  
 C Schematic representation of VISP1 substitution mutants in the UIM and ARM regions. UIM: ubiquitin-interacting motif, ARM: arginine/lysine-rich motif.  
 D BiFC assays analyzing interactions between VISP1 and SGS3 or its deletion mutants in *N. benthamiana* leaves. Scale bar = 20 μm.  
 E BiFC assays analyzing interactions between SGS3 and VISP1, VISP1<sup>mUIM</sup>, or VISP1<sup>mARM</sup> in *N. benthamiana* leaves. Scale bar = 20 μm.  
 F Co-immunoprecipitation analyses of the interactions between SGS3, SGS3<sup>ACC</sup>, or SGS3<sup>CC</sup> and VISP1 or VISP1<sup>mARM</sup>. *N. benthamiana* leaves were agroinfiltrated with constructs as indicated and treated with 2 mM 3-MA at 48 hpi and collected for IP with anti-Flag beads 12 h later.  
 G GST pull-down analysis of the *in vitro* interactions of SGS3<sup>CC</sup> with VISP1, VISP1<sup>mARM</sup>, or VISP1<sup>mUIM</sup>. GST-VISP1, GST-VISP1<sup>mARM</sup>, GST-VISP1<sup>mUIM</sup> or GST were incubated with SGS3<sup>CC</sup>-His for IP with anti-GST beads and detected by Western blotting with GST or His antibodies.

Source data are available online for this figure.

were individually mutated and fused to Y<sup>C</sup> (Fig 5C). The BiFC results revealed that SGS, SGS3<sup>ΔN</sup>, and SGS3<sup>ΔXS</sup>, but not SGS3<sup>ΔCC</sup>, interacted with VISP1 (Fig 5D and Appendix Fig S10B). In addition, co-expression of SGS3-Y<sup>N</sup> with VISP1-Y<sup>C</sup> and VISP1<sup>mUIM</sup>-Y<sup>C</sup>, but not with VISP1<sup>mARM</sup>-Y<sup>C</sup> resulted in reconstitution of YFP signal (Fig 5E and Appendix Fig S10C). Collectively, these results reveal that the VISP1–SGS3 interaction requires the SGS3 CC domain and the VISP1 ARM motif.

Co-IP assays were performed to validate the VISP1–SGS3 interaction in vivo. In this experiment, VISP1-GFP, VISP1<sup>mARM</sup>-GFP, VISP1<sup>mUIM</sup>-GFP, or GFP were co-expressed with SGS3-Flag, SGS3<sup>ΔCC</sup>-Flag, or SGS3<sup>CC</sup>-Flag in *N. benthamiana* leaves through agroinfiltration. To inhibit autophagy-mediated SGS3 degradation, co-infiltrated *N. benthamiana* leaves were treated with 2 mM 3-MA at 48 hpi and collected for immunoprecipitation with anti-Flag beads 12 h later. Western blotting revealed that VISP1-GFP, rather than VISP1<sup>mARM</sup>-GFP or GFP, was precipitated with SGS3-Flag (Fig 5F). Moreover, SGS3<sup>CC</sup>-Flag, but not SGS3<sup>ΔCC</sup>-Flag, could be associated with VISP1-GFP (Fig 5F). We next examined the direct VISP1–SGS3 interaction using pull-down assays. Since the full-length SGS3 protein was difficult to be expressed in *E. coli*, we fused the SGS3 CC domain with a 6 × His tag and purified the SGS3<sup>CC</sup>-His protein. The results reveal that the SGS3<sup>CC</sup>-His protein was precipitated with GST-VISP1 and GST-VISP1<sup>mUIM</sup>, but not with GST-VISP1<sup>mARM</sup> or GST (Fig 5G).

Collectively, our results demonstrate that VISP1 interacts directly with the CC domain of SGS3 in vivo and in vitro. Together with the results above (Fig 1), these results suggest that VISP1 exploits two different motifs, ARM and UIM, to interact with the SGS3 cargo and ATG8, respectively.

### VISP1 mediates autophagic degradation of SGS3/RDR6 bodies

To determine whether VISP1 acted as a cargo receptor of SGS3, we examined whether VISP1 drove SGS3 into autophagosomes through co-expressing VISP1-GFP, RFP-SGS3, and CFP-NbATG8f (Wang et al, 2013). Upon treatment with E64d, VISP1-GFP and RFP-SGS3

were co-localized with CFP-NbATG8f-labeled autophagosomes in agroinfiltrated cells (Fig 6A). Furthermore, co-expression of SGS3-Y<sup>N</sup>/VISP1-Y<sup>C</sup> formed YFP granules that were co-localized with CFP-NbATG8f-labeled autophagosomes (Fig 6B). Numbers of these co-localized granules increased strikingly upon treatment with E64d (Fig 6B). Co-expression of SGS3<sup>ΔCC</sup>-Y<sup>N</sup>/VISP1-Y<sup>C</sup> as a negative control did not form YFP-labeled granules (Fig 6B). These results suggest that VISP1 and SGS3 are associated with ATG8-labeled autophagosomes.

To further determine VISP1-mediated degradation of SGS3, both SGS3-Flag and SGS3<sup>ΔCC</sup>-Flag were co-expressed with VISP1-Flag in *N. benthamiana* leaves. At 60 hpi, accumulation of SGS3-Flag in the presence of VISP1-Flag reduced to approximately 10% of that of the empty vector (EV)-treated leaves (Fig 6C). Furthermore, 3-MA treatment rescued accumulation of SGS3-Flag to about 73% (Fig 6C). Semi-quantity RT-PCR revealed that VISP1 did not affect SGS3 mRNA levels (Fig 6C). SGS3<sup>ΔCC</sup>-Flag was not affected by VISP1, because SGS3<sup>ΔCC</sup>-Flag does not interact with VISP1 (Fig 6C). Further degradation analyses revealed that accumulation of SGS3-Flag was not affected by either VISP1<sup>mARM</sup> or VISP1<sup>mUIM</sup> that did not interact with SGS3 or ATG8 (Fig 6D and E). Collectively, these results indicate that both VISP1–SGS3 and VISP1–ATG8 interactions are essential for VISP1-mediated autophagic degradation of SGS3.

In plants, SGS3 and RDR6 form SGS3/RDR6 bodies that are required for siRNA amplification (Wang et al, 2010; Dong et al, 2016). Co-expression of SGS3-Y<sup>N</sup>/VISP1-Y<sup>C</sup> constituted YFP-labeled granules that were co-localized with RDR6-RFP (Appendix Fig S11A), indicating that SGS3 bridged SGS3/RDR6 bodies with VISP1. Moreover, the numbers of RDR6/SGS3 bodies formed by RDR6-Y<sup>N</sup>/SGS3-Y<sup>C</sup> obviously decreased in the presence of VISP1-Flag (Fig 6F and G). Western blotting showed that accumulation of RDR6-Y<sup>N</sup> and SGS3-Y<sup>C</sup> in VISP1-Flag samples was lower than that of EV samples (Fig 6H). The E64d and 3-MA treatments abolished VISP1-mediated degradation of RDR6/SGS3 bodies (Appendix Fig S11B and C). Moreover, neither VISP1<sup>mARM</sup>-Flag nor VISP1<sup>mUIM</sup>-Flag affected the RDR6/SGS3-body numbers or accumulation of RDR6-Y<sup>N</sup> and SGS3-Y<sup>C</sup> proteins (Fig 6F and G, and H). Therefore, these

**Figure 6. VISP1 mediates selective autophagic degradation of SGS3/RDR6 bodies.**

- A Confocal analysis of co-localization of VISP1-GFP and RFP-SGS3 with the CFP-NbATG8f-labeled autophagic bodies in *N. benthamiana* leaves. The infiltrated leaves were treated with 100 μM E64d or DMSO at 48 hpi and examined at 60 hpi. Arrow heads indicate autophagic bodies. Scale bar = 10 μm.
- B Confocal analysis of co-localization of CFP-NbATG8f-labeled autophagic bodies with the VISP1-Y<sup>N</sup> and SGS3-Y<sup>C</sup> bodies in *N. benthamiana* leaves. The infiltrated leaves were treated with 100 μM E64d or DMSO at 48 hpi and examined for imaging at 60 hpi. Scale bar = 20 μm.
- C Effect of VISP1-Flag and the autophagy inhibitor 3-MA on accumulation of SGS3-Flag and SGS3<sup>ΔCC</sup>-Flag in *N. benthamiana* leaves. The co-infiltrated leaves were treated with 3-MA (10 mM) or buffer at 48 hpi and were harvested for western blotting 12 h later. Accumulation of AtSGS3 transcript was analyzed by RT-PCR.
- D Effect of VISP1<sup>mARM</sup>-Flag on accumulation of SGS3-Flag.
- E Effect of VISP1<sup>mUIM</sup>-Flag on accumulation of SGS3-Flag.
- F Confocal analysis of effect of VISP1-Flag, VISP1<sup>mARM</sup>-Flag, and VISP1<sup>mUIM</sup>-Flag on RDR6-Y<sup>N</sup> and SGS3-Y<sup>C</sup> formed bodies in *N. benthamiana* leaves at 60 hpi. EV: empty vector. Scale bar = 20 μm.
- G Numbers of RDR6-Y<sup>N</sup> and SGS3-Y<sup>C</sup> formed bodies per 10 cells in (E) were used for quantification. Data points represent means of three biological repeats. Error bars indicate SD. Letters indicate significant differences (ANOVA,  $P < 0.05$ ).
- H Western blotting showing accumulation of proteins as indicated in the samples of (E).
- I Western blotting detecting accumulation of the endogenous SGS3 protein in leaves of 2-week-old Col-0, VISP1<sup>OE</sup>, *uisp1*, and *sgs3-1 Arabidopsis* plants with anti-SGS3 antibodies.
- J Western blotting detecting accumulation of the endogenous SGS3 protein in leaves of 2-week-old Col-0, VISP1<sup>OE</sup>, VISP1<sup>mUIM/OE</sup>, and VISP1<sup>mARM/OE Arabidopsis</sup> plants.
- K Western blotting detecting accumulation of the endogenous SGS3 protein in 2-week-old VISP1-overexpressing Col-0, *atg5-1*, and *atg7-1* mutants.

Data information: EV, empty vector. (B–D) Relative accumulation (RA) represents means ± SD from band densities in three biological repeats. (C–E, H) RbCl served as loading controls. (I–K) Actin served as a loading control. Source data are available online for this figure.



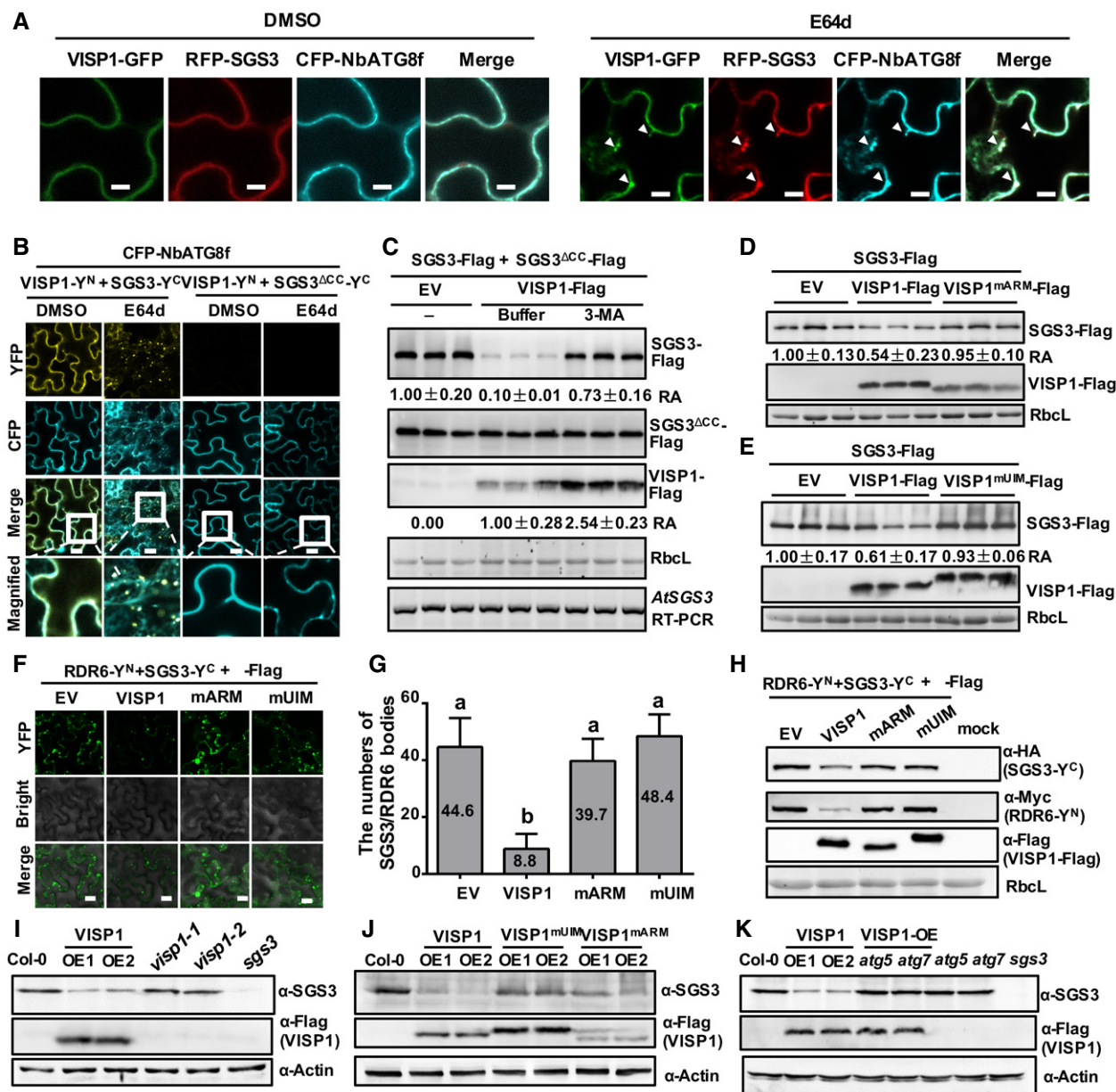


Figure 6.

results indicate that the SGS3/RDR6 bodies are degraded cargos of VISP1 in vivo.

We further examined endogenous SGS3 accumulation in Col-0, VISP1<sup>OE</sup>, VISP1<sup>mUIM/OE</sup>, VISP1<sup>mARM/OE</sup>, and *visp1* mutants with anti-SGS3 antibodies. Accumulation of SGS3 decreased in VISP1<sup>OE</sup> plants compared with that of Col-0 plants (Fig 6I). In contrast, VISP1<sup>mUIM</sup> and VISP1<sup>mARM</sup> overexpression had less effect on SGS3 accumulation (Fig 6J). In consistence, overexpression of VISP1<sup>mUIM</sup> and VISP1<sup>mARM</sup> did not affect antiviral immunity in transgenic plants (Appendix Fig S12). Furthermore, overexpression of VISP1 had no effect on accumulation of endogenous SGS3 protein in the background of *atg5-1* and *atg7-3* mutants (Fig 6K), indicating that VISP1 mediates degradation of SGS3 through autophagy pathway. Collectively, these results suggest that VISP1

triggers selective autophagic turnover of SGS3/RDR6 bodies in plants.

#### VISP1 negatively regulates biogenesis of endogenous tasiRNAs

We next examined whether VISP1 inhibited endogenous trans-acting siRNA (tasiRNAs) that have been shown to be dependent on SGS3 and RDR6 (Peragine *et al*, 2004). Firstly, 5-week-old VISP1<sup>OE</sup> seedlings, mimicking *sgs3-1* developmental phenotype, had downwardly curled rosette leaves (Fig 7A), which represents accelerated transition from juvenile to adult phase as described previously (Peragine *et al*, 2004; Xie *et al*, 2005). The length/width ratios of rosette leaves from VISP1<sup>OE1</sup>, VISP1<sup>OE2</sup>, and *sgs3-1* mutants were significantly (*P*-value < 0.01) higher than those of

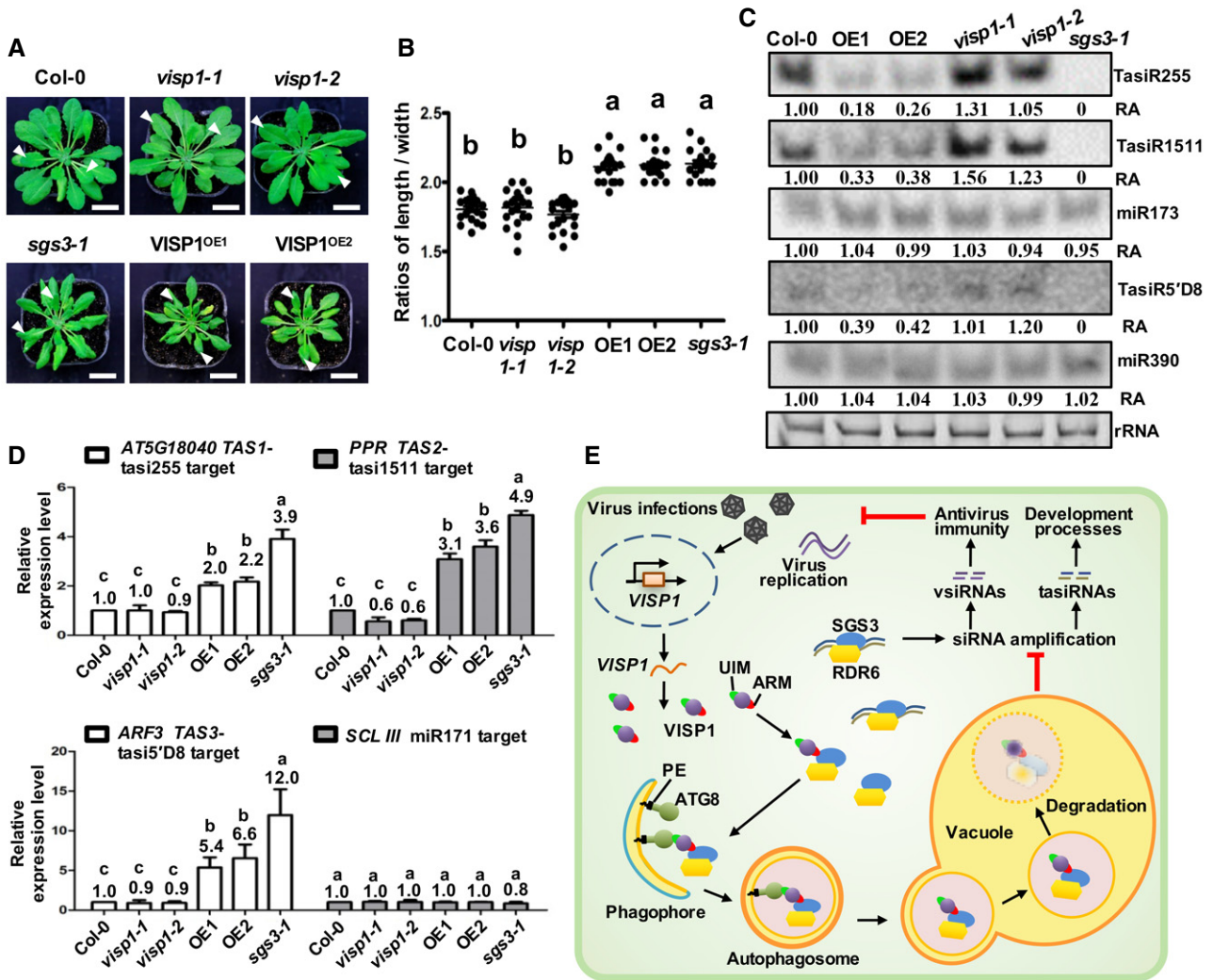


**Figure 7. VISP1 negatively affects tasiRNA biogenesis.**

- A** Developmental phenotypes of rosette leaves of 5-week-old Col-0, *visp1-1*, *visp1-2*, *VISP1*<sup>OE1</sup>, *VISP1*<sup>OE2</sup>, and *sgs3-1* seedlings. Arrowheads indicate the 8<sup>th</sup> and 9<sup>th</sup> rosette leaves from the top leaves. Scale bar = 2 cm.
- B** The length/width ratios of the 8<sup>th</sup> and 9<sup>th</sup> rosette leaves of the seedlings shown in (A). Every dot represents data from the length/width ratio of one leaf ( $n = 20$ ). Letters indicate significant differences (ANOVA,  $P < 0.05$ ).
- C** Northern blotting detecting accumulation of TAS1-TasiR255, TAS2-TasiR1511, TAS3-TasiR5'D8, miR173, and miR390 in leaves of *Arabidopsis* plants shown in panel (A). Values represent relative accumulation (RA) of siRNAs, and values in Col-0 plants were set as 1. rRNA served as loading controls.
- D** RT-qPCR analyzing accumulation of TAS-tasiRNA targets in rosette leaves of 4-week-old *Arabidopsis* plants. Values in Col-0 plants were set as 1. Data points represent means from three biological repeats. Error bars indicate SD. Letters indicate significant differences (ANOVA,  $P < 0.05$ ). PPR, pentatricopeptide repeat (PPR); ARF3, auxin response factor 3.
- E** Model of VISP1-mediated autophagic degradation of SGS3/RDR6 bodies in *Arabidopsis*. SGS3/RDR6 bodies mediate dsRNA synthesis for siRNA amplification. Virus infection induces overexpression of VISP1 and selective autophagy. VISP1, a cargo receptor, interacts with SGS3 via the VISP1 arginine/lysine-rich motif (ARM) and recruits SGS3/RDR6 bodies to ATG8-PE docking site through the VISP1 ubiquitin-interacting motif (UIM). This then promotes selective autophagic degradation of SGS3/RDR6 bodies and negatively regulates amplification of vsirRNAs and tasiRNA.

Source data are available online for this figure.

counterpart leaves in Col-0, *visp1-1*, and *visp1-2* plants (Fig 7B). In contrast, VISP1 overexpression in the background of *atg5-1* and *atg7-3* mutants did not induce *sgs3-1* developmental phenotype (Appendix Fig S13). Indeed, RDR6, SGS3, and the tasiRNA pathway have been shown to play a role in vegetative phase change (Peragine *et al.*, 2004). Therefore, these results suggest that VISP1-mediated autophagy affects vegetative phase change

through degrading SGS3/RDR6 and down-regulating endogenous tasiRNAs.

Northern blotting was performed to evaluate whether VISP1 affected biogenesis of tasiRNAs. As expected, tasiR255 and tasiR1511, respectively from TAS1 and TAS2, accumulated to markedly lower levels in two *VISP1*<sup>OE</sup> lines but to relative higher levels in two *visp1* mutants compared with those of Col-0 plants (Fig 7C).

Hybridization signal intensities of tasiRNAs analyses revealed that accumulation of tasiR255 and tasiR1511 reduced to 18%–38% in *VISP<sup>OE</sup>* lines and increased to 120–150% in *visp1* mutants compared with that of Col-0 plants (Fig 7C). In contrast, these plants accumulated similar levels of miR173 that is responsible for initial cleavage of the *TAS* precursors (Fig 7C). Similarly, *VISP1* negatively regulated accumulation of the *TAS3*-derived tasiR5'D8 but did not affect that of the upstream miR390 (Fig 7C). Collectively, these results demonstrate that *VISP1* inhibits biogenesis of tasiRNAs through degrading SGS3/RDR6 bodies.

In previous studies, tasiRNAs accumulated to low levels and tasiRNA target transcripts accumulated to relatively high levels in *sgs3-1* mutant plants (Vazquez et al, 2004; Allen et al, 2005). RT-qPCR assays were carried out to measure transcript levels of tasiRNA target genes in plants. *VISP1* and SGS3 did not affect miRNA activity because accumulation of the miR171-targeting gene was comparable in these plants (Fig 7D). In contrast, all tasiRNA targets, including the *TAS1*-tasi255-targeting *AT5G18040*, the *TAS2*-tasi1511-targeting *pentatricopeptide repeat (PPR)*, and *TAS3*-tasi5'D8-targeting *auxin response factor 3 (ARF3)*, were significantly up-regulated in *VISP<sup>OE1</sup>*, *VISP<sup>OE2</sup>*, and *sgs3-1* plants and reduced in *visp1-1* and *visp1-2* compared with those of Col-0 plants (Fig 7D). Collectively, *VISP1* inhibits biogenesis of endogenous tasiRNAs and thereby up-regulates accumulation of the tasiRNA targets.

In conclusion, our results demonstrate that *VISP1* is a virus-optimized cargo receptor involved in autophagic degradation of SGS3/RDR6 bodies, thereby inhibiting antiviral silencing and tasiRNA pathways (Fig 7E).

## Discussion

Nearly 8,000 sORFs harboring 30–100 amino acids were predicted from the *Arabidopsis* genome (Hanada et al, 2013); however, few studies have conducted to explore their functions. The main aim of this study was to seek sORF functions in plant virus infection. We exploited transcriptional analyses of *Arabidopsis* peptidome and identified 18 virus-induced sORF mRNAs. Furthermore, we demonstrated that *VISP1* could be translated in vivo using GUS fusion assays. Through genetic and biochemical analyses, we clearly revealed that *VISP1* was a functional peptide in crosstalk of selective autophagy and RNA silencing. Identification of new receptors or adaptors is important for exploring the functions of selective autophagy. In addition to the well-studied ATG8-interacting motif (AIM), the ubiquitin-interacting motif (UIM) is recently highlighted as a conserved motif in ATG8-binding adaptors and receptors (Marshall et al, 2019). Here, we have characterized *VISP1* as a new UIM-containing receptor through showing the direct *VISP1*–ATG8 interaction, which is dependent on the *VISP1* UIM motif. Thus, the small peptide *VISP1* and homologues represent a new class autophagy cargo receptor with UIM domain.

We further identified SGS3/RDR6 bodies as the cargos of *VISP1*. SGS3/RDR6 bodies are critical components during amplification of vsRNAs and endogenous tasiRNAs (Vazquez et al, 2004; Wang et al, 2010). Since SGS3/RDR6 bodies dependent endogenous tasiRNAs have important roles in plant development (Xie et al, 2005; Marin et al, 2010), their homeostasis must be finely regulated during plant development. Thus, *VISP1* is responsible for tuning

down SGS3/RDR6-dependent pathways to avoid constitutive induction. When *VISP1* is induced by stresses or plant development, like *VISP1<sup>OE</sup>* lines, plants will exhibit dwarf and narrow leaves mimicking *sgs3* and *rdr6* mutants (Fig 7). In addition to involvement in plant development, RDR6/SGS3 bodies have essential roles in vsRNA amplification and innate immunity against plant viruses. Thus, their homeostasis is usually manipulated by plant viruses or other plant components. The potyvirus VPg protein and the *N. benthamiana* endogenous NbCaM interact with SGS3 and trigger autophagic degradation of SGS3 (Cheng & Wang, 2017; Li et al, 2017). However, these studies failed to identify the involved selective receptors and the underlying mechanisms (Ismayil et al, 2019). Here, our results fill the gap that *VISP1* is a new virus co-opted cargo receptor regulating autophagic degradation of SGS3 and RDR6, and thereby facilitates virus infection (Figs 3 and 4). Further study is required to determine other cargo proteins of *VISP1* as well as their functions in development and/or stress processes.

Another significant finding of this study is that *visp1* mutants exhibit normal developmental phenotypes and potent antiviral immunity against different viruses (Fig 4). Host factors required for plant virus infection can serve as recessive resistant genes for breeding antiviral plants. In previous studies, the isoforms of eukaryotic translation initiation factor (eIF) 4E and eIF4G have been used as recessive resistance genes in genetic-modified crops against potyviruses (Truniger & Aranda, 2009; Hashimoto et al, 2016). Nonetheless, utility of eIF4E and eIF4G only confers resistance against limited plant viruses. Since RDR6 and SGS3 are conserved components in antiviral silencing, *VISP1* knockout probably mediates broad-spectrum resistance to plant viruses. Thus, our results imply that *VISP1* is a promising target for genome editing in antiviral crop breeding.

In summary, we have identified that *VISP1* is a new peptide cargo receptor targeting SGS3/RDR6 bodies for autophagic degradation. Our findings fill the gap in understanding homeostasis regulation of SGS3/RDR6 bodies by selective autophagy. Moreover, our results highlight a new important function of small peptide with 30–100 amino acids in the crosstalk between RNA silencing and selective autophagy.

## Materials and Methods

### Plant materials

All *Arabidopsis* wild-type, overexpression, knockout and mutant plants are in the Col-0 background. The mutants *rdr6-15* (SAIL\_617\_H07), *sgs3-1*, *atg5-1* (SAIL\_129B07), *atg7-3* (SAIL\_11H07) were described previously (Thompson et al, 2005; Lai et al, 2011; Dong et al, 2016; Luo et al, 2017; Guo et al, 2018). The pMDC32-*VISP1*, pMDC32-*VISP1<sup>mUIM</sup>*, and pMDC32-*VISP1<sup>mARM</sup>* plasmids were generated by introducing the *VISP1*, *VISP1<sup>mUIM</sup>*, and *VISP1<sup>mARM</sup>* ORFs into the pMDC32 vector (Curtis & Grossniklaus, 2003) and then transformed in Col-0 plants to obtain *VISP1*, *VISP1<sup>mUIM</sup>*, and *VISP1<sup>mARM</sup>* overexpression lines. The pMDC32-*VISP1* was transformed in *atg5-1* and *atg7-3* plants to generate *VISP<sup>OE</sup>/atg5-1* and *VISP<sup>OE</sup>/atg7-3* lines. To generate *visp1* mutant lines, two 19-bp guide sequences were inserted into pHEC401 vector (Xing et al, 2014) and then transformed into Col-0 plants, and two independent *visp1* lines containing 104- and 105-nucleotide deletion were obtained

(Appendix Fig S8), respectively. The YFP-ATG8e marker in pBI121 vector has been described previously (Zhuang *et al*, 2013). The pBI-YFP-ATG8e was further transformed into Col-0 and VISP1<sup>OE</sup> plants to label autophagy bodies. Note that all the unlabeled ATG8 proteins were from *Arabidopsis* except for the *N. benthamiana* ATG8f protein in the CFP-NbATG8f plasmid (Wang *et al*, 2013). Primers for the generation of these constructs are listed in Appendix Table S1.

### Growth conditions and virus infection

*Arabidopsis thaliana* seedlings were plated on MS medium (Caisson Laboratories, Rexburg, ID) supplemented with 3% sucrose and 1.2% agar with pH 5.8–6.0. Seedlings were vernalized in dark at 4°C for 3–4 days and then grown in soil at 22–23°C with a 10/14-h light/dark cycle. For nitrogen starvation, seeds were germinated on 1/2 MS medium for 4 days and then transferred to 1/2 MS medium without nitrogen (Caisson Laboratories, 01160003) for 3 days. Three expanded leaves of four-week-old seedlings were mechanically inoculated with CMV (20 ng/μl) or CMV-2blm (30 ng/μl) as described previously (Dong *et al*, 2016; Zhang *et al*, 2019). Systemically infected leaves were collected for protein and RNA analyses at 14 or 21 dpi. *N. benthamiana* plants were grown in a growth room with a controlled condition at 25°C under a 14/10 h light/dark cycle.

### Transcriptional data analyses

The transcriptome data from mock- and CMV-treated plants were aligned to the reference genome ([http://plants.ensembl.org/Arabidopsis\\_thaliana/Info/Index](http://plants.ensembl.org/Arabidopsis_thaliana/Info/Index)) of *A. thaliana* using tophat2 (Kim *et al*, 2013) with the parameter of N3-i60-I6000-p16-read-edit-dist 3. Custom bed files containing TAIR10 gene structure annotation and sORF gene structure annotation information (Hanada *et al*, 2013) were used to calculate RPKM for comparing expression level of genes and sORFs by the method of RSeQC (v2.6) (Wang *et al*, 2012; Wang *et al*, 2016). Differential expression levels were analyzed with edgeR package (Robinson *et al*, 2010; McCarthy *et al*, 2012). In the edgeR results, FDR < 0.05 was set as the thresholds to identify differentially expressed genes. Differentially expressed sORFs further filtered by log<sub>2</sub> fold-change > 2 to identify significantly up-regulated sORFs.

### Western blotting analysis

To generate the anti-SGS3 antibodies, the cDNA fragment corresponding to the C terminus of the *Arabidopsis* SGS3 protein (aa 297–625) was cloned into pET30a (+) vector. The SGS3 fragment was expressed and purified from *E. coli* with Ni-NTA agarose (QIAGEN). Then, the purified SGS3 protein (aa 297–625) was used to immunize rabbits to obtain polyclonal antibodies against the *Arabidopsis* SGS3 protein (Beijing Genomics institution, China). Western blotting analyses were performed as described previously (Fang *et al*, 2019). Total proteins were extracted in SDS buffer [100 mM Tris (pH 6.8), 4% SDS, 20% glycerol, and 0.2% bromophenol blue, 10% β-mercaptoethanol], separated in SDS-PAGE, and transferred to nitrocellulose membranes. The GFP, CMV CP, SGS3, Flag-tagged, GST-tagged, and His-tagged proteins were detected with anti-GFP (1:1,000), anti-CP (1:3,000), anti-SGS3(1:1,000), anti-Flag (1:5,000,

Sigma) monoclonal antibodies, anti-GST (1:10,000, Abcam), and anti-His (1:5,000, Proteintech) monoclonal antibodies, respectively. The membranes were incubated with goat anti-rabbit or mouse IgG conjugated with horseradish peroxidase (Bio-Rad, 1:20,000) and detected by Bio-Rad imaging system. For detection of ATG8a-PE, SDS-PAGE with 6 M urea was performed as described previously (Yang *et al*, 2019). Polyclonal antibodies against ATG8a (1:1,000, ab77003) were purchased from Abcam.

### BiFC assays and subcellular localization

Bimolecular fluorescence complementation (BiFC) assays were performed as described previously (Li *et al*, 2017). The ORFs of VISP1, SGS3, RDR6, ATG7, ATG8, and their derived mutants were cloned in-frame with the N- or C-terminal halves of YFP in the pSPYNE-35S or pSPYCE-35S vectors (Walter *et al*, 2004). Note that the YFP N halve was fused to the N terminus of ATG8a to avoid degradation by autophagy. *A. tumefaciens* EHA105 strains containing BiFC plasmid combinations and the tomato bushy stunt virus P19 plasmid were co-infiltrated into *N. benthamiana* leaves at a ratio of 0.4:0.4:0.2 (OD600). At 60 h post-inoculation (hpi), YFP fluorescence of epidermal cells of infiltrated patches was examined by Zeiss LSM 710 confocal microscope with excitation wavelength of 514 nm and emission wavelength of 525–555 nm. For co-localization with RDR6-RFP and CFP-NbATG8f, RFP and CFP were monitored with excitation wavelengths of 561 and 440 nm, respectively. Besides, light emitted at 633 nm was used to record chloroplast II auto-fluorescence.

### Detection of SGS3 accumulation in *N. benthamiana* leaves

SGS3-Flag and SGS3<sup>ACC</sup>-Flag were co-expressed with VISP1 or its mutant in *N. benthamiana* leaves by *Agrobacterium* infiltration as described previously (Zhang *et al*, 2017). At 2 dpi, the leaves were infiltrated with water or 10 mM 3-MA (AbMole) for 12 h and then detected accumulation of SGS3-Flag and VISP1-Flag using Western blotting analyses with anti-Flag antibody.

### GUS staining

GUS staining assays were performed as described previously (Zhang *et al*, 2019). To clone the *VISP1* promoter, the genomic region between 3.0 kb upstream of the start codon of *VISP1* and the stop codon was inserted into the pBI101 vector (Clontech). The resulting plasmids harboring *VISP1*<sup>PRO</sup>::*VISP1*-GUS and *VISP1*<sup>PRO</sup>::*VISP1*<sup>TGA</sup>-GUS were transformed into Col-0 plants via *A. tumefaciens*. The infected plants were vacuumed twice in GUS staining buffer (3 mM X-Gluc, 50 mM NaH<sub>2</sub>PO<sub>4</sub> buffer, pH 7.0, 10 mM potassium ferrocyanide, 10 mM potassium ferricyanide, 0.5% β-mercaptoethanol, and 0.1% Triton X-100) for 10 min and then inoculated in dark at 37°C for 14 h. After washed with a 70% ethanol series, the stained plants were photographed with a digital camera.

### Identification of *VISP1* fragments by LC-MS/MS

Total proteins were extracted from systemically infected leaves of *VISP1*<sup>PRO</sup>::*VISP1*-GUS transgenic plants infected with CMV at 7 dpi. The supernatant was incubated with 10 μg anti-GUS antibodies for

1 h at room temperature and then added 30  $\mu$ l washed Pierce™ Protein A/G magnetic beads at room temperature for 1 h. After washed 3 times, the beads were boiled to isolate protein for SDS–PAGE electrophoresis. After stained by silver stain kit (Sigma–Aldrich), the VISP1–GUS band was sliced and digested with trypsin at 37°C overnight. The digested peptides were then analyzed by the Mass Spectrometry Facility of China Agricultural University by Orbitrap Fusion Lmuos LC–MS/MS (Thermo Scientific, Waltham, MA, USA).

### Monodansylcadaverine (MDC) staining and microscopy

*Arabidopsis* seedlings were stained with MDC solution as described previously (Yang et al, 2018). Briefly, 7-day-old seedlings were treated with DTT, NaCl, and virus infection and immersed in 0.05 mM MDC solution for 10 min in dark. After washed 4 times with phosphate-buffered saline (PBS) buffer, MDC fluorescence of seedlings was observed using a Zeiss LSM710 confocal microscope (Carl Zeiss) with a 4', 6-diamidino-2-phenylindole (DAPI)-specific filter.

### Chemical treatments and TEM

Chemical treatments and TEM observation were performed as described previously (Yang et al, 2018). For *Arabidopsis*, 4-week-old mock or CMV-2blm infected leaves were infiltrated with 1  $\mu$ M ConA (Aladdin) at 4 dpi for 12 h in dark. For *N. benthamiana*, leaves expressing transiently VISP1–Flag were treated with 100  $\mu$ M E64d (Selleck) in dark at 48 hpi and collected for observation of autophagic bodies using TEM at 60 hpi. Leaves were cut into small pieces (~2 mm<sup>2</sup>) and vacuum-infiltrated in 0.05 M phosphate buffer (pH 7.0) containing 2.5% glutaraldehyde. The samples were then post-fixed in 2% OsO<sub>4</sub>, dehydrated in ethanol and acetone, and then embedded in Spurr's resin (SPI Supplies). Ultrathin sections (70 nm) were cut with a diamond knife on an ultramicrotome (EM UC7; Leica) and collected on copper grids and then stained with uranyl acetate and lead citrate before final examination under an electron microscope (Hitachi, h-7650b).

### RNA analyses

RNA analyses were carried out as described previously (Zhang et al, 2019). Briefly, total RNA was isolated from systemic leaves of 15–20 *Arabidopsis* plants with Trizol reagent (Invitrogen, USA). For RT–qPCR analysis, 2.5  $\mu$ g total RNA was treated with DNase I and then acted as templates to synthesize first-strand cDNAs with M–MLV reverse transcriptase (Promega, USA). qPCR assays were carried out with the SsoFast™ EvaGreen® Supermix (Bio–Rad) and specific primers listed in Appendix Table S2. The *Arabidopsis Actin2* gene served as an endogenous control. For northern blotting assays, systemically infected or mock *Arabidopsis* leaves of 20–30 plants were pooled for RNA extraction. High (5  $\mu$ g) and low (15  $\mu$ g) molecular RNAs were used to detect viral RNAs and siRNAs, respectively, as described previously (Wang et al, 2010). For detection of CMV genomic and sgRNAs, cDNA amplified from the 3' terminus 240 nt of Fny–CMV–RNA2 was randomly labeled with [ $\alpha$ -<sup>32</sup>P] dCTP. Small RNAs were detected by the [ $\gamma$ -<sup>32</sup>P] ATP-labeled DNA oligonucleotides for detection of vsRNAs, miR173, tasi255, and tasi1511 listed in Appendix Table S2 as described previously (Allen et al, 2005; Wang et al, 2011).

### In vivo coimmunoprecipitation (Co-IP) assays

The Co-IP assays were performed as described previously (Zhang et al, 2020). The ORFs of SGS3, mutants, and ATG8a were introduced into the pMDC32 vector for expressing SGS3–Flag, SGS3<sup>CC</sup>–Flag, and Flag–ATG8a transiently in *N. benthamiana* leaves. The VISP1 and its mutants were cloned into pGDm vector for expression of VISP1–GFP, VISP1<sup>mARM</sup>–GFP, and VISP1<sup>mUIM1</sup>–GFP. Co-IP assays were performed as described previously (Zhang et al, 2017). *N. benthamiana* leaves were agroinfiltrated for expressing SGS3–Flag, Flag–ATG8a, VISP1–GFP, and GFP in different combinations, treated with 10 mM 3-MA at 2 dpi, and then harvested for Co-IP assays 12 h later. Approximately 3 g of infiltrated leaves was homogenized in extraction buffer (10% [v/v] glycerol, 50 mM Tris–HCl, pH 7.5, 1 mM EDTA, 100 mM NaCl, 0.1% NP-40, 2% PVP-40, 10 mM DTT, 1  $\times$  cocktail) and centrifuged at 13,523 g for 40 min at 4°C. The resulting supernatant was incubated with pre-equilibrated and BSA blocked anti-Flag M2 agarose beads (Sigma–Aldrich, USA) for 4 h at 4°C. The beads were washed three times with IP buffer, and the beads bound proteins were detected using Western blotting assays with anti-GFP (1:1,500) and anti-FLAG (1:3,000) monoclonal antibodies, respectively.

### GST pull-down assays

The GST pull-down assays were performed as described previously (Gao et al, 2020). For GST pull-down assay, the ORFs of ATG8a, VISP1, VISP1<sup>mARM</sup>, and VISP1<sup>mUIM1</sup> were cloned into pGEX–KG to express GST–ATG8a, GST–VISP1, GST–VISP1<sup>mARM</sup>, and GST–VISP1<sup>mUIM1</sup>. The coding sequences of SGS3<sup>CC</sup>, VISP1, and its mutants were engineered into pET30a (+) for expression of SGS3<sup>CC</sup>–His, VISP1–His, VISP1<sup>mARM</sup>–His, and VISP1<sup>mUIM1</sup>–His, respectively. All resulting recombinant plasmids were introduced into *E. coli* BL21 for protein expression. GST pull-down assays were performed as described previously (Yang et al, 2018). In binding assays, 10  $\mu$ g of bait and prey proteins was incubated with GST beads in 500  $\mu$ l binding buffer [20 mM Tris–HCl (pH 7.5), 100 mM NaCl, 0.6% (v/v) Triton X-100, 1 Mm PMSF, 0.2% (v/v) glycerol, and 10 mM DTT] at 4°C for 4 h. After washing six times with washing buffer [50 mM Tris–HCl (pH 7.5), 400 mM NaCl and 0.6% (v/v) Triton X-100], bound proteins on beads were eluted by boiling in 60  $\mu$ l 2 $\times$  SDS–PAGE loading buffer and subjected to SDS–PAGE analyzed by anti-His or GST antibody.

### Quantification and statistical analysis

All experiments were repeated at least 3 times, and representative results are shown. For all assays, means and standard deviation (SD) values were calculated, and significances were determined by Student's *t*-test or ANOVA followed by Tukey's multiple comparison test.

### Accession numbers

Genes used in this study can be found in GenBank/EMBL libraries under the following accession numbers: *AtVISP1* (MT063056), *AtATG5* (NM\_121735.5), *AtATG7* (NM\_123958.3), *AtATG8a* (NM\_001084955.1), *AtATG8f* (NM\_117751.4), *AtATG12* (NM\_001333633.1),

*AtSGS3* (NM\_122263), *AtRDR6* (NM\_001339423.1), *NbATG8f* (KU561372.1), *Actin2* (AY096381.1), *CMV-RNA1* (NC\_002034.1); *CMV-RNA2* (NC\_002035.1), *CMV-RNA3* (NC\_001440.1); the protein accession number of *VISP1* orthologues are EFH69431.1, KFK44251.1, VDD37223.1, RQL81863.1, VVA92088.1, RID53695.1, CDY38808.1, VVB02607.1, RID58242.1, VDD37176.1.

## Data availability

RNA-Seq data: Gene Expression Omnibus PRJNA575609 (<https://www.ncbi.nlm.nih.gov/bioproject/PRJNA575609>).

**Expanded View** for this article is available online.

## Acknowledgments

We thank our colleagues Jialin Yu, Dawei Li, and Yongliang Zhang for their helpful discussion. We thank Savithramma P. Dinesh-Kumar (University of California at Davis) for constructive criticism. We thank Yule Liu (Tsinghua University) for providing the CFP-NbATG8f plasmid. We thank Xiangfeng Wang (China Agricultural University, College of Biological Sciences) for providing the pBI-YFP-ATG8e plasmid. We thank Qingqiu Gong (Nankai University) for providing the *atg5-1* and *atg7-3* mutants. Research in Wang laboratory is supported by Natural Science Foundation of China (31872920 and 31571978) and the Fundamental Research Funds for the Central Universities (CAU, 2020TC163).

## Author contributions

XT performed the majority of the experiments, assisted by SL, JZ, JZ, FZ, LC, XT, and SL, and XW analyzed the data. XW and XT wrote the manuscript, assisted by YW and CH. All authors discussed the results and commented on the manuscript.

## Conflict of interest

The authors declare that they have no conflict of interest.

## References

- Allen E, Xie Z, Gustafson AM, Carrington JC (2005) MicroRNA-directed phasing during trans-acting siRNA biogenesis in plants. *Cell* 121: 207–221
- Cheng X, Wang A (2017) The Potyvirus silencing suppressor protein VPg mediates degradation of *SGS3* via ubiquitination and autophagy pathways. *J Virol* 91: 01478–16
- Curtis MD, Grossniklaus U (2003) A gateway cloning vector set for high-throughput functional analysis of genes in planta. *Plant Physiol* 133: 462–469
- De Smet R, Sabaghian E, Li Z, Saeys Y, Van de Peer Y (2017) Coordinated functional divergence of genes after genome duplication in *Arabidopsis thaliana*. *Plant Cell* 29: 2786–2800
- Diaz-Pendon JA, Li F, Li W-X, Ding S-W (2007) Suppression of antiviral silencing by Cucumber mosaic virus 2b protein in *Arabidopsis* is associated with drastically reduced accumulation of three classes of viral small interfering RNAs. *Plant Cell* 19: 2053–2063
- Dong K, Wang Y, Zhang Z, Chai LX, Tong X, Xu J, Li D, Wang XB (2016) Two amino acids near the N terminus of cucumber mosaic virus 2b play critical roles in the suppression of RNA silencing and viral infectivity. *Mol Plant Pathol* 17: 173–183
- Fang XD, Yan T, Gao Q, Cao Q, Gao DM, Xu WY, Zhang ZJ, Ding ZH, Wang XB (2019) A cytorhabdovirus phosphoprotein forms mobile inclusions trafficked on the actin/ER network for viral RNA synthesis. *J Exp Bot* 70: 4049–4062
- Gao Q, Yan T, Zhang Z-J, Liu S-Y, Fang X-D, Gao D-M, Yang Y-Z, Xu W-Y, Qiao J-H, Cao Q et al (2020) Casein kinase 1 regulates cytorhabdovirus replication and transcription by phosphorylating a phosphoprotein serine-rich motif. *Plant Cell* 32: 2878–2897
- Guo Z, Li Y, Ding SW (2019) Small RNA-based antimicrobial immunity. *Nat Rev Immunol* 19: 31–44
- Guo Z, Lu J, Wang X, Zhan B, Li W, Ding SW (2017) Lipid flippases promote antiviral silencing and the biogenesis of viral and host siRNAs in *Arabidopsis*. *Proc Natl Acad Sci USA* 114: 1377–1382
- Guo Z, Wang XB, Wang Y, Li WX, Gal-On A, Ding SW (2018) Identification of a new host factor required for antiviral RNAi and amplification of viral siRNAs. *Plant Physiol* 176: 1587–1597
- Hanada K, Higuchi-Takeuchi M, Okamoto M, Yoshizumi T, Shimizu M, Nakaminami K, Nishi R, Ohashi C, Iida K, Tanaka M et al (2013) Small open reading frames associated with morphogenesis are hidden in plant genomes. *Proc Natl Acad Sci USA* 110: 2395–2400
- Hashimoto M, Neriya Y, Yamaji Y, Namba S (2016) Recessive resistance to plant viruses: potential resistance genes beyond translation initiation factors. *Front Microbiol* 7: 1695
- Ichimura Y, Kirisako T, Takao T, Satomi Y, Shimonishi Y, Ishihara N, Mizushima N, Tanida I, Kominami E, Ohsumi M et al (2000) A ubiquitin-like system mediates protein lipidation. *Nature* 408: 488–492
- Ismayil A, Yang M, Liu Y (2019) Role of autophagy during plant-virus interactions. *Semin Cell Dev Biol* 101: 36–40
- Kim D, Perteau G, Trapnell C, Pimentel H, Kelley R, Salzberg SL (2013) TopHat2: accurate alignment of transcriptomes in the presence of insertions, deletions and gene fusions. *Genome Biol* 14: R36
- Kirkin V, Lamark T, Sou YS, Bjorkoy G, Nunn JL, Bruun JA, Shvets E, McEwan DG, Clausen TH, Wild P et al (2009) A role for NBR1 in autophagosomal degradation of ubiquitinated substrates. *Mol Cell* 33: 505–516
- Lai Z, Wang F, Zheng Z, Fan B, Chen Z (2011) A critical role of autophagy in plant resistance to necrotrophic fungal pathogens. *Plant J* 66: 953–968
- Li F, Zhao N, Li Z, Xu X, Wang Y, Yang X, Liu S-S, Wang A, Zhou X (2017) A calmodulin-like protein suppresses RNA silencing and promotes geminivirus infection by degrading *SGS3* via the autophagy pathway in *Nicotiana benthamiana*. *PLoS Pathog* 13: e1006213
- Luo L, Zhang P, Zhu R, Fu J, Su J, Zheng J, Wang Z, Wang D, Gong Q (2017) Autophagy is rapidly induced by salt stress and is required for salt tolerance in *Arabidopsis*. *Front Plant Sci* 8: 1459
- Marin E, Jouannet V, Herz A, Lokerse AS, Weijers D, Vaucheret H, Nussaume L, Crespi MD, Maizel A (2010) miR390, *Arabidopsis* TAS3 tasiRNAs, and their AUXIN RESPONSE FACTOR targets define an autoregulatory network quantitatively regulating lateral root growth. *Plant Cell* 22: 1104–1117
- Marshall RS, Hua Z, Mali S, McLoughlin F, Vierstra RD (2019) ATG8-binding UIM proteins define a new class of autophagy adaptors and receptors. *Cell* 177: 766–781
- Marshall RS, Li F, Gemperline DC, Book AJ, Vierstra RD (2015) Autophagic degradation of the 26S proteasome is mediated by the dual ATG8/ubiquitin receptor RPN10 in *Arabidopsis*. *Mol Cell* 58: 1053–1066
- Marshall RS, Vierstra RD (2018) Autophagy: the master of bulk and selective recycling. *Annu Rev Plant Biol* 69: 173–208
- McCarthy DJ, Chen Y, Smyth GK (2012) Differential expression analysis of multifactor RNA-Seq experiments with respect to biological variation. *Nucleic Acids Res* 40: 4288–4297

- Michaeli S, Honig A, Levanony H, Peled-Zehavi H, Galili G (2014) Arabidopsis ATG8-INTERACTING PROTEIN1 is involved in autophagy-dependent vesicular trafficking of plastid proteins to the vacuole. *Plant Cell* 26: 4084–4101
- Mourrain P, Béclin C, Elmayan T, Feuerbach F, Godon C, Morel J-B, Jouette D, Lacombe A-M, Nikic S, Picault NJC (2000) Arabidopsis SGS2 and SGS3 genes are required for posttranscriptional gene silencing and natural virus resistance. *Cell* 101: 533–542
- Noda NN, Ohsumi Y, Inagaki FJFI (2010) Atg8-family interacting motif crucial for selective autophagy. *FEBS Lett* 584: 1379–1385
- Olsson V, Joos L, Zhu S, Gevaert K, Butenko MA, De Smet I (2018) Look closely, the beautiful may be small: precursor-derived peptides in plants. *Annu Rev Plant Biol* 70: 153–186
- Pankiv S, Clausen TH, Lamark T, Brech A, Bruun JA, Outzen H, Overvatn A, Bjorkoy G, Johansen T (2007) p62/SQSTM1 binds directly to Atg8/LC3 to facilitate degradation of ubiquitinated protein aggregates by autophagy. *J Biol Chem* 282: 24131–24145
- Peragine A, Yoshikawa M, Wu G, Albrecht HL, Poethig RS (2004) SGS3 and SGS2/SDE1/RDR6 are required for juvenile development and the production of trans-acting siRNAs in Arabidopsis. *Genes Dev* 18: 2368–2379
- Robinson MD, McCarthy DJ, Smyth GK (2010) edgeR: a Bioconductor package for differential expression analysis of digital gene expression data. *Bioinformatics* 26: 139–140
- Signorelli S, Tarkowski ŁP, Van den Ende W, Bassham DC (2019) Linking autophagy to abiotic and biotic stress responses. *Trends Plant Sci* 24: 413–430
- Svenning S, Lamark T, Krause K, Johansen T (2011) Plant NBR1 is a selective autophagy substrate and a functional hybrid of the mammalian autophagic adapters NBR1 and p62/SQSTM1. *Autophagy* 7: 993–1010
- Tavormina P, De Coninck B, Nikonorova N, De Smet I, Cammue BP (2015) The plant peptidome: an expanding repertoire of structural features and biological functions. *Plant Cell* 27: 2095–2118
- Thompson AR, Doelling JH, Suttangkakul A, Vierstra RD (2005) Autophagic nutrient recycling in Arabidopsis directed by the ATG8 and ATG12 conjugation pathways. *Plant Physiol* 138: 2097–2110
- Truniger V, Aranda MA (2009) Recessive resistance to plant viruses. *Adv Virus Res* 75: 119–159
- Vazquez F, Vaucheret H, Rajagopalan R, Lepers C, Gascioli V, Mallory AC, Hilbert JL, Bartel DP, Crete P (2004) Endogenous trans-acting siRNAs regulate the accumulation of Arabidopsis mRNAs. *Mol Cell* 16: 69–79
- Walter M, Chaban C, Schutze K, Batistic O, Weckermann K, Nake C, Blazevic D, Grefen C, Schumacher K, Oecking C et al (2004) Visualization of protein interactions in living plant cells using bimolecular fluorescence complementation. *Plant J* 40: 428–438
- Wang L, Nie J, Sicotte H, Li Y, Eckel-Passow JE, Dasari S, Vedell PT, Barman P, Wang L, Weinshiboum R et al (2016) Measure transcript integrity using RNA-seq data. *BMC Bioinformatics* 17: 58
- Wang L, Wang S, Li W (2012) RSeQC: quality control of RNA-seq experiments. *Bioinformatics* 28: 2184–2185
- Wang P, Mugume Y, Bassham DC (2018) New advances in autophagy in plants: regulation, selectivity and function. *Semin Cell Dev Biol* 80: 113–122
- Wang XB, Jovel J, Udornporn P, Wang Y, Wu Q, Li WX, Gascioli V, Vaucheret H, Ding SW (2011) The 21-nucleotide, but not 22-nucleotide, viral secondary small interfering RNAs direct potent antiviral defense by two cooperative argonautes in *Arabidopsis thaliana*. *Plant Cell* 23: 1625–1638
- Wang XB, Wu Q, Ito T, Cillo F, Li WX, Chen X, Yu JL, Ding SW (2010) RNAi-mediated viral immunity requires amplification of virus-derived siRNAs in *Arabidopsis thaliana*. *Proc Natl Acad Sci USA* 107: 484–489
- Wang Y, Yu B, Zhao J, Guo J, Li Y, Han S, Huang L, Du Y, Hong Y, Tang D et al (2013) Autophagy contributes to leaf starch degradation. *Plant Cell* 25: 1383–1399
- Xie Z, Allen E, Wilken A, Carrington JC (2005) DICER-LIKE 4 functions in trans-acting small interfering RNA biogenesis and vegetative phase change in *Arabidopsis thaliana*. *Proc Natl Acad Sci USA* 102: 12984–12989
- Xing HL, Dong L, Wang ZP, Zhang HY, Han CY, Liu B, Wang XC, Chen QJ (2014) A CRISPR/Cas9 toolkit for multiplex genome editing in plants. *BMC Plant Biol* 14: 327
- Yang F, Kimberlin AN, Elowsky CG, Liu Y, Gonzalez-Solis A, Cahoon EB, Alfano JR (2019) A plant immune receptor degraded by selective autophagy. *Mol Plant* 12: 113–123
- Yang M, Ismayil A, Liu Y (2020) Autophagy in plant-virus interactions. *Annu Rev Virol* 7: 403–419
- Yang M, Zhang Y, Xie X, Yue N, Li J, Wang X-B, Han C, Yu J, Liu Y, Li D (2018) Barley stripe mosaic virus  $\gamma$ b protein subverts autophagy to promote viral infection by disrupting the ATG7-ATG8 interaction. *Plant Cell* 30: 1582–1595
- Zhang X-P, Liu D-S, Yan T, Fang X-D, Dong K, Xu J, Wang Y, Yu J-L, Wang XB (2017) Cucumber mosaic virus coat protein modulates the accumulation of 2b protein and antiviral silencing that causes symptom recovery in plants. *PLoS Pathog* 13: e1006522
- Zhang ZJ, Gao Q, Fang XD, Ding ZH, Gao DM, Xu WY, Cao Q, Qiao JH, Yang YZ, Han C et al (2020) CCR4, a RNA decay factor, is hijacked by a plant cytorhabdovirus phosphoprotein to facilitate virus replication. *eLife* 9: e53753
- Zhang Z, Tong X, Liu SY, Chai LX, Zhu FF, Zhang XP, Zou JZ, Wang XB (2019) Genetic analysis of a Piezo-like protein suppressing systemic movement of plant viruses in *Arabidopsis thaliana*. *Sci Rep* 9: 3187
- Zhou J, Wang J, Cheng Y, Chi YJ, Fan B, Yu JQ, Chen Z (2013) NBR1-mediated selective autophagy targets insoluble ubiquitinated protein aggregates in plant stress responses. *PLoS Genet* 9: e1003196
- Zhou J, Wang Z, Wang X, Li X, Zhang Z, Fan B, Zhu C, Chen Z (2018) Dicot-specific ATG8-interacting AT13 proteins interact with conserved UBAC2 proteins and play critical roles in plant stress responses. *Autophagy* 14: 487–504
- Zhuang X, Chung KP, Cui Y, Lin W, Gao C, Kang B-H, Jiang L (2017) ATG9 regulates autophagosome progression from the endoplasmic reticulum in *Arabidopsis*. *Proc Natl Acad Sci USA* 114: E426–E435
- Zhuang X, Wang H, Lam SK, Gao C, Wang X, Cai Y, Jiang L (2013) A BAR-domain protein SH3P2, which binds to phosphatidylinositol 3-phosphate and ATG8, regulates autophagosome formation in *Arabidopsis*. *Plant Cell* 25: 4596–4615